Composites Science and Technology 210 (2021) 108793

Contents lists available at ScienceDirect

Composites Science and Technology

journal homepage: http://www.elsevier.com/locate/compscitech

# Polymer beads as interfacial obstacles in fibre composites

Carol W. Rodricks, Israel Greenfeld, H. Daniel Wagner *

*Department of Materials and Interfaces, Weizmann Institute of Science, Israel*

ARTICLE INFO

*Keywords:*
Interface
Beaded fibre composite
Structural modification
Mechanical interlocking

ABSTRACT

The geometric modification of fibre-matrix interfaces is a promising approach for simultaneous improvement of strength and toughness of composites. In this study, we investigate the effect of discrete epoxy droplets deposited on glass fibres embedded in an epoxy matrix, using single fibre experiments. Pullout tests reveal increases in both the pullout force and work in beaded fibre samples compared to beadless ones. This is somewhat unexpected as the bead and the matrix are made of the same material (cured epoxy) and possess the same mechanical properties. Interestingly, upon pullout, only the fibres are extracted from the matrix whereas the beads remain within the matrix, indicating that failure occurs at the fibre-bead interface. The simultaneous improvement in pullout force and work seen during the pullout of beaded fibres is explained by a conceptual anchoring mechanism based on friction lock, which agrees well with the experimental results. Smaller beads yield higher increases in pullout force and work, leading to the possibility of denser packing of multiple beaded fibres in a practical composite.

## 1. Introduction

Engineering structural materials are required to be strong and tough, yet these properties are often mutually exclusive of each other and the simultaneous improvement of both strength and toughness in such materials is a challenge [1–3]. In fibre-reinforced composites, the interface plays an important role in the balance between strength and toughness. For instance, strong bonds at the interface ensure good stress transfer from the matrix to the fibre and result in a strong but typically brittle composite, whereas weaker bonds at the interface allow for energy dissipation and redistribution of stress around cracks and defects, resulting in a tough, yet usually weak composite [4]. Various studies have explored chemical modification of the interface through coupling agents to improve the overall mechanical properties of a composite, but improvement of one property is usually accompanied by the degradation of the other [5–7].

Natural composites, on the other hand, rarely depend solely on the chemical or material properties of their constituents, but make use of the physical geometry of constituents for an optimised balance of strength and toughness [8,9]. Mechanical interlocking at interfaces plays as important a role as the nature of bonding between constituents, as seen in nacre [10], bone [1,11], wood and bamboo [2] and bird feathers [12,13]. The mechanical properties of natural composites far exceed the sum of their parts. The structural design of constituents is therefore a promising tactic towards achieving a superior balance of strength and toughness, and a number of studies over the years that focus on the mechanical interlocking of constituents in synthetic composites [3,14–21] supports this hypothesis.

Here we continue an investigation into a one such structural design – epoxy beads at the interface of fibre-reinforced composites [14,15]. Epoxy droplets are deposited along the surface of a glass fibre, resulting in a fibre with an undulating topography. The working hypothesis is that the strength of a composite made from such fibres improves due to the beads acting as anchors for better stress transfer from the matrix to the fibre when the composite is under load. The toughness improves through increased energy dissipation due to higher resistance to fibre pullout, and due to plastic deformation of the surrounding matrix and, possibly, of the beads themselves [14]. A similar structure of intermittently spaced topographical anchors is found in the rachis (shaft) of a bird's feather [12,13]. The 'nodules' in the feather improve the transmission of forces (strength) and increase the pull-out resistance of the fibre (toughness) [12] – precisely what the intermittently spaced beaded fibres are hypothesised to do.

In the current study we explore the effect of the interlocking of beads through pullout tests of single beaded fibres. Fibres with a single bead are embedded and then pulled out from a matrix, and the pullout work and maximum force are measured as functions of the fibre embedded depth and the bead size. A model glass fibre-epoxy system is studied, where the beads and the matrix are of the same material. To rule out material effects, the properties of the bead and matrix materials are

* Corresponding author.
*E-mail address:* daniel.wagner@weizmann.ac.il (H.D. Wagner).

https://doi.org/10.1016/j.compscitech.2021.108793
Received 17 November 2020; Received in revised form 21 March 2021; Accepted 28 March 2021
Available online 3 April 2021

compared by Differential Scanning Calorimetry (DSC) analysis and mechanical tests. Micro-computer tomography (μCT) is used to view the debonding morphology, and the effective interfacial shear strength (IFSS) is calculated using the Cottrell-Kelly-Tyson approach [22–24]. A phenomenological mechanical model based on friction lock is put forth to describe the pullout mechanism of single beaded fibres in more detail.

## 2. Experimental

### 2.1. Materials

The fibres used in this study were E-glass fibres (S139, Vetrotex International Saint-Gobain) with an average diameter of 18 μm. Surface impurities were removed by rinsing the fibres several times in acetone before drying them in an oven for 1 h at 80 °C. The beads on the fibres and the matrix were both made from the same epoxy. EP828, a bisphenol-A diglycidyl ether and a compatible polyetheramine hardener, EPC304, were the chosen epoxy system and were both supplied by Polymer Gvulot Ltd., Israel. The resin and hardener were mixed in a weight ratio of 100:42 using a centrifugal mixer with deaeration capabilities (Thinky ARE-250 CE) to ensure a homogenous epoxy mixture free of air bubbles. The curing cycle of the epoxy was 6 h at 100 °C.

### 2.2. Beaded fibre preparation

Beaded fibres were prepared by depositing epoxy droplets on E-glass fibres. Glass fibres were gently stretched taut and glued to a metal frame using masking tape (Fig. 1a). They were then suspended vertically and a drop of epoxy (post mixing and deaeration) was deposited on each fibre using a fragment of another glass fibre. The drop was allowed to slide down the fibre under gravity, depositing a thin uniform layer of epoxy onto the surface of the fibre. This layer spontaneously and almost instantaneously partitioned into uniformly spaced, almost identical droplets along the length of the fibre as a result of the Plateau-Rayleigh instability phenomenon [14,15] (Fig. 1b). A description of the process and the instability phenomenon can be found in Ref. [14]. The fibres with the epoxy beads were then moved to an oven and cured for 6 h at 100 °C.

It is possible to control the size (length and diameter) and wavelength of the beads by controlling the thickness of the layer of epoxy deposited on the fibre. A thicker layer would result in larger beads and longer wavelength. The thickness of the epoxy layer can in turn be controlled by the size, viscosity and surface tension of the initial droplet of epoxy applied on the fibre. A more viscous droplet would result in a thicker coating, and consequently, larger beads with longer wavelengths, as would a larger initial droplet. A smaller, or less viscous droplet would result in a thinner coating of epoxy on a fibre and therefore smaller beads. More detail can be found in Ref. [14]. In an alternative approach [15], dip-coating of fibres in an epoxy bath was used as a successful means of controlling the beading parameters. In this method, the resin viscosity and surface tension and the speed at which the fibres are drawn out of the epoxy bath affect the thickness of the epoxy layer on the fibre, which in turn affects the bead. Higher viscosity and drawout velocity would result in a thicker epoxy layer, which would result in bigger beads with longer wavelengths, and vice versa [15].

### 2.3. Single fibre tensile tests

Single fibre tensile tests were performed on beaded fibres and the results were compared to E-glass fibres with no beads (the control). Three fibre gauge lengths of 10 mm, 30 mm and 50 mm were used. Tensile tests were carried out on an Instron (model 5965) at a rate of 1 μm $s^{-1}$.

### 2.4. Single fibre pullout test

The effect of a single bead at the interface of a fibre was investigated through the single fibre pullout test. Tests were performed on single end bead fibres and compared to fibres without epoxy beads (the control).

#### 2.4.1. Sample preparation for pullout test

Fibres were embedded in liquid epoxy using a custom-made heating device that consisted of two orthogonal microcallipers, a heating element and a rotating platform (Fig. 2a). The horizontal microcalliper and the rotating platform allowed for the positioning of the fibre, and the vertical calliper was used to control the length to which a fibre was embedded. Liquid epoxy was held in a metal screw cap that fitted into the heating element. The set-up allowed the liquid epoxy to be cured partially before the sample was moved to an oven for the full cure cycle.

End-beaded fibres were made by cutting long multi-beaded fibres under an optical microscope using a scalpel. The fibres were cut in such a way that a bead was as close to the end of the fibre fragment as possible (Fig. 2b). The dimensions of the end beads were measured under the optical microscope. The bead diameters on beaded fibres tested in this study ranged from 23 μm to 61 μm, and had corresponding lengths of 49 μm–120 μm. The embedded lengths of beaded fibres ranged 56 μm–189 μm and were measured as the span of the fibre inside the bead plus the remaining portion of the fibre in the matrix (Fig. 2c).

Embedded lengths lower than 56 μm were not attempted due to the minimum bead length being 49 μm. Lower embedded lengths would have resulted in the beads protruding out from the epoxy matrix instead of being completely embedded in it. A higher range of embedded lengths of 25 μm–200 μm was, however, possible for beadless fibres. Once a fibre was embedded in liquid epoxy placed in the heating device, the epoxy

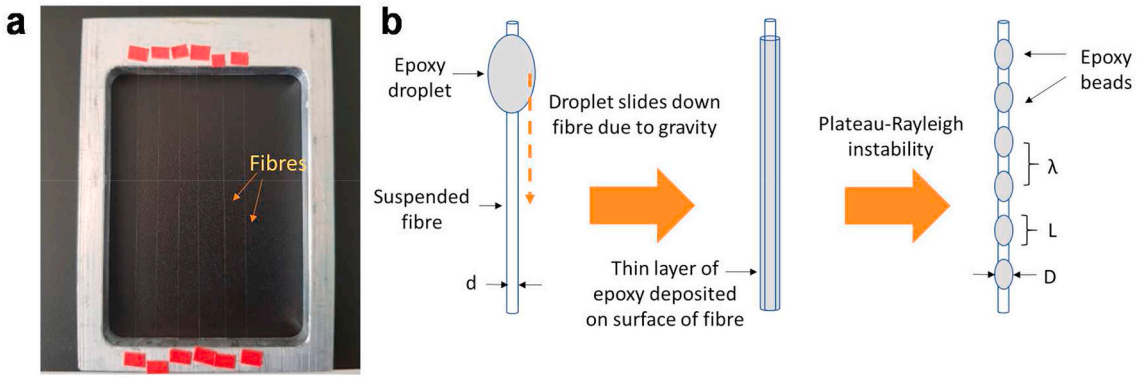


**Fig. 1. Preparation of beaded fibres**. (a) Metal frame with suspended fibres. (b) Formation of intermittent beads on fibre through Plateau-Rayleigh instability [14,15]. A droplet of epoxy is placed on a fibre of diameter $d$ and allowed to slide down the fibre resulting in a thin layer of epoxy which spontaneously breaks into uniformly spaced beads of length $L$, diameter $D$ and wavelength $\lambda$.

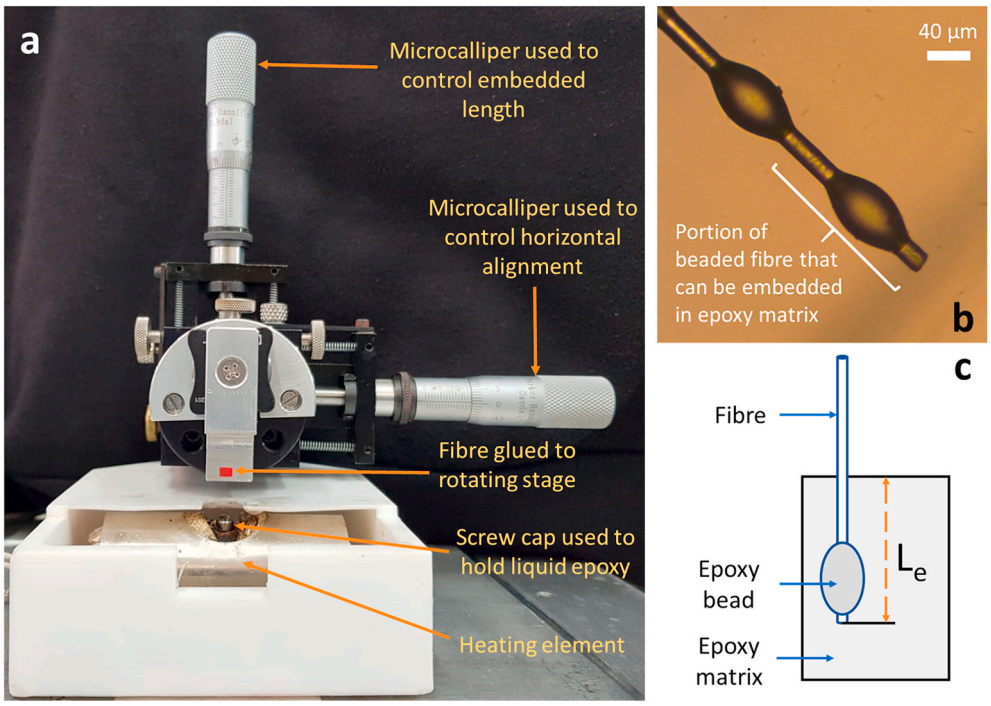


**Fig. 2. Sample preparation for single fibre pullout tests.** (a) Embedding device used to insert fibre in epoxy to a desired embedded length. (b) Beaded fibre cut under an optical microscope to obtain a bead at the end of the fibre. Only a single bead is embedded in epoxy for the tests. (c) Schematic diagram of pullout sample defining the embedded length $L_e$.

was partially cured for 30 min at 100 °C until it was solid enough to hold the fibre in place. The fibre was then cut from the stage, and the screw cap with the epoxy and fibre was transferred to an oven where the sample was cured for 5 h and 30 min at 100 °C, making the total cure time of the epoxy matrix 6 h at 100 °C.

### 2.4.2. *Pullout test*

The single fibre pullout test was performed on a homemade assembly designed in house, that consisted of a piezo-actuator (Physik Instrumente GmbH, Germany), a load cell (Kistler, Switzerland) and a high voltage amplifier. The crosshead movement range was 180 µm and the system was calibrated to measure forces withing a range of 0–80 N. The components of the assembly were mounted on a steel frame to ensure a sufficiently stiff setup to avoid deflection during the pullout of the beaded fibres.

The screw with the embedded fibre was threaded into the main socket of the load cell (Fig. 3). The free end of the fibre was glued directly to the actuator using a stiff cyanoacrylate glue (CN, Tokyo Measuring Instruments laboratory, Japan). The glue was stiff enough when dry to securely hold the free end of the fibre in place during pullout, and therefore no clamps or paper tabs were needed. Due to the presence of beads on the free end of beaded fibres, the free length of the fibre could not be kept constant, but was within the range of 50 µm–100 µm. The rate at which the fibre was pulled out was kept constant at 1 µm $s^{-1}$.

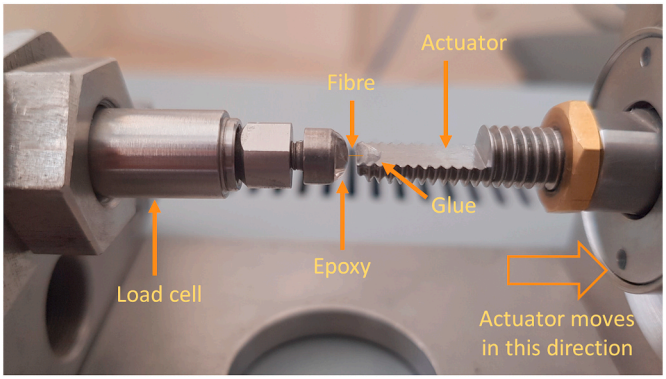


**Fig. 3. Set-up for pullout test of single fibres.**

## 2.5. *Epoxy characterisation*

To understand the effect of the cure cycle on epoxy properties, characterisation tests were carried out on bulk epoxy that was cured through two different cure cycles to emulate the bead curing. The components of the epoxy resin were mixed, deaerated and poured into silicon moulds to make dog-bone shaped samples. The uncured epoxy samples were separated into two batches. The first batch of epoxy was cured once for 6 h at 100 °C. These one-time-cure samples were labelled SCE (single cure epoxy). The second batch of epoxy was first cured for 6 h at 100 °C, then allowed to stand at room temperature for 24 h before it was cured a second time for 6 h at 100 °C. These samples were labelled as DCE (double cure epoxy). The dog-bone shaped samples had a cross-section of 1 × 1.5 $mm^2$ and a gauge length of 12 mm.

### 2.5.1. *Matrix tensile tests*

Tensile tests were done to determine any changes in the mechanical properties of the epoxy matrix. The tensile tests were carried out on the dog-bone shaped samples of SCE and DCE on a Minimat tensile tester with a 200 N load cell and at a rate of 1 µm $s^{-1}$.

### 2.5.2. *Differential Scanning Calorimetry (DSC)*

Differential scanning calorimetry (DSC) was done on the SCE and DCE samples to monitor changes in properties of epoxy as a function of its curing cycle. The instrument used for the measurements was a TA Instruments DSC Q200. Tests were run on SCE (4.7 mg) and DCE (4.9 mg) in hermetically sealed aluminium crucibles under nitrogen and with a ramp rate of 10 °C $min^{-1}$. The temperature range for the tests was 40 °C–400 °C.

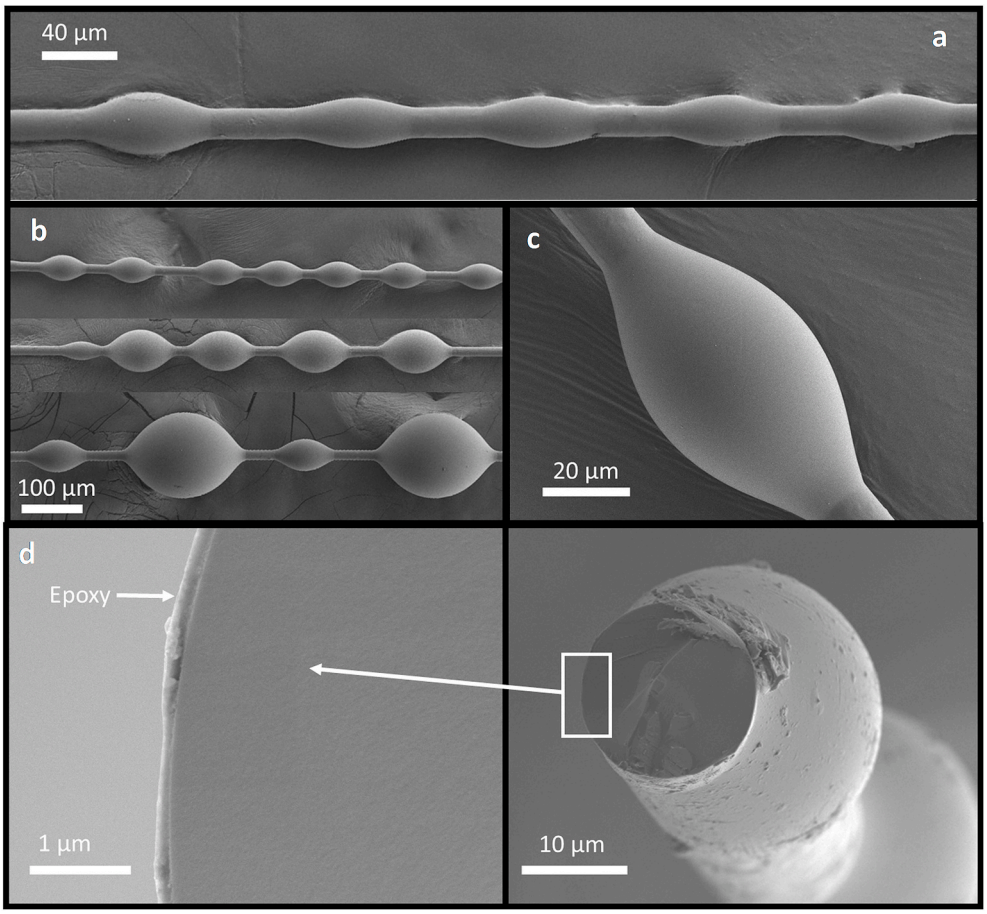


**Fig. 4. SEM images of cured EP828 epoxy beads on E-glass fibres**. (a–b) Beaded fibres with beads of various diameters. Alternating large and small beads are seen when bead diameter > 70 µm. (c) Surface of bead. (d) Beaded fibre cut between beads. A thin epoxy film is seen on the surface of the fibre.

## 3. Results and discussion

### 3.1. Beaded fibre dimensions

Beaded fibres with various bead shapes and sizes are presented in Fig. 4. We see that the beads are fairly uniformly sized and spaced and that the surface of the beads is smooth (Fig. 4c). A thin epoxy layer of 100 nm–200 nm thickness is seen on the fibre between the beads (Fig. 4d). For larger bead sizes, smaller beads are seen to alternate between bigger beads (bead diameter >70 µm), as in Fig. 4b. This happens when the epoxy layer between the bigger beads is sufficiently thick for a secondary instability to form, resulting in the alternating smaller beads. The smallest bead diameter possible with the method described in section 2.2 was 23 µm, with a corresponding length of 49 µm, and the largest bead diameter possible without the secondary instability was about 70 µm, with a corresponding bead length of 130 µm.

### 3.2. Beaded fibre strength and stiffness

Single fibre tensile tests were performed on beaded fibres to study the effect of the beads on fibre strength. The beads as well as the thin layer of epoxy between beads could potentially quench defects on the surface of fibres and thus improve fibre strength. Tensile test results of beaded fibre were compared to plain glass fibres which were free of beads and epoxy, as seen in Table 1.

A slight reduction was observed in the modulus of the beaded fibres as compared to the fibres with no beads, but the elongation to failure and tensile strength were not significantly different. Physical modifications of a fibre's surface, such as through etching, usually result in fibre strength degradation, even if the interfacial adhesion to the matrix is enhanced [11,20,25], but here the tensile strength is neither improved nor degraded due to the presence of the beads. Epoxy beads at the interface therefore appear to be a promising method of modifying a fibre surface without compromising on its strength.

### 3.3. Pullout force and work; effective interfacial shear strength

Pullout tests were performed to investigate the effect of the beads at the interface of a fibre. A single bead at the end of a beaded fibre was embedded in a matrix and pulled out using the test method described in

**Table 1**
Single fibre tensile test at fibre length of 50 mm, 30 mm and 10 mm – beaded fibres vs. fibres with no beads (control).

| Fibre | Modulus (GPa) | Elongation to failure (Strain %) | Tensile strength (MPa) | | |
|---|---|---|---|---|---|
| | | | 50 mm | 30 mm | 10 mm |
| **Fibre (no bead)** | 68.5 ± 3.7 | 2.6 ± 0.6 | 1685 ± 381 | 1881 ± 455 | 1985 ± 295 |
| **Beaded fibre** | 67.2 ± 3.6 | 3.0 ± 0.7 | 1484 ± 403 | 1817 ± 400 | 2034 ± 433 |
| **p-value (T-Test)** | 0.03 | 0.43 | 0.14 | 0.60 | 0.46 |

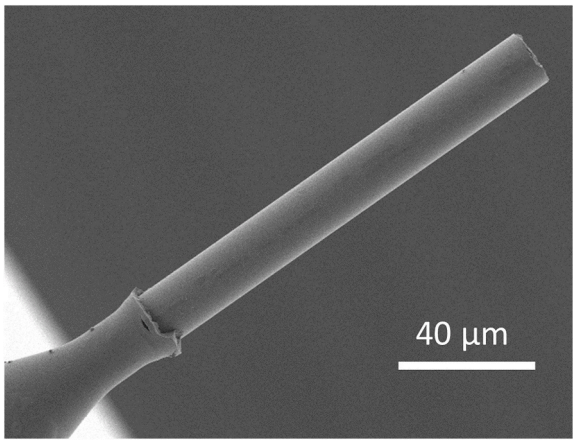


**Fig. 5. Beaded fibre after pullout**. No epoxy residue left on fibre surface.

section 2.4. The results were compared to the pullout results of plain glass fibres without beads (*i.e.*, the control). None of the beaded fibre samples pulled out with the bead – the fibre-matrix interface failed for all beaded fibre samples and the bead remained in the matrix, while the fibre was pulled out (Fig. 5). No epoxy residue remained on the surface of the fibres that pulled out and the failure was adhesive and brittle. Beaded fibres with bead diameters greater than 60 µm typically broke rather than pulled out and therefore tests with beads of higher diameters were not performed.

Force-displacement graphs of beaded fibres compared to beadless fibres at embedded lengths of 145 ± 10 µm are presented in Fig. 6a. The pullout travel of a beaded fibre typically consisted of four consecutive segments: a first elastic segment of length ~5–25 µm, similar to that of a beadless fibre; a second elastic segment of length ~5–25 µm, with a slightly lower slope and a higher peak stress; a short plastic segment of length ~1–5 µm, maintaining the same peak stress; and a steep stress drop due to fibre debonding, followed by a long friction segment that runs until complete pullout. The second elastic segment, which is unique to beaded fibres, is the predominant contribution to the increase in pullout work with respect to beadless fibres (Fig. 6d). Beaded fibres were seen to have higher maximum pullout forces and longer displacements as compared to beadless fibres. The frictional contribution from the beaded fibres (*i.e.*, the low force region), when the debonded fibre is pulled through the matrix and bead, appears to be similar to the beadless fibres. This was expected as the bead was not pulled out from the matrix and so the frictional contribution for the beaded fibres was purely from the fibre being pulled through the epoxy after debonding from the bead and the matrix.

The maximum pullout force for several beaded fibres is depicted as a function of the embedded length in Fig. 6b. It was generally seen that beaded fibres had higher maximum pullout forces compared to beadless fibres at the same embedded length. The beaded fibre data had more scatter that was likely due to the bead diameter variation as a range of bead diameters was used in this test. The increase in the pullout force of the beaded fibres implies that the beads anchored the fibres in the matrix. The beads appear to add a delta-force of 0.146 N, which can be thought of as the net contribution of the bead to $F_{max}$.

The dependence of the interfacial shear strength of the beaded fibres and the beadless fibres on the embedded length is plotted in Fig. 6c. The calculation of the interfacial shear strength ($\tau$) was done using the Cottrell-Kelly-Tyson (CKT) model [22–24] which assumes constant $\tau$ along the interface of the fibre. $\tau$ was calculated using Equation (1), where $F_{max}$ is the maximum pullout force, $d$ the fibre diameter and $L_e$ the embedded length of the fibre. $\tau$ calculated using this approach is therefore an average or effective value of the interfacial stresses.

$$\tau = \frac{F_{max}}{\pi d L_e} \tag{1}$$

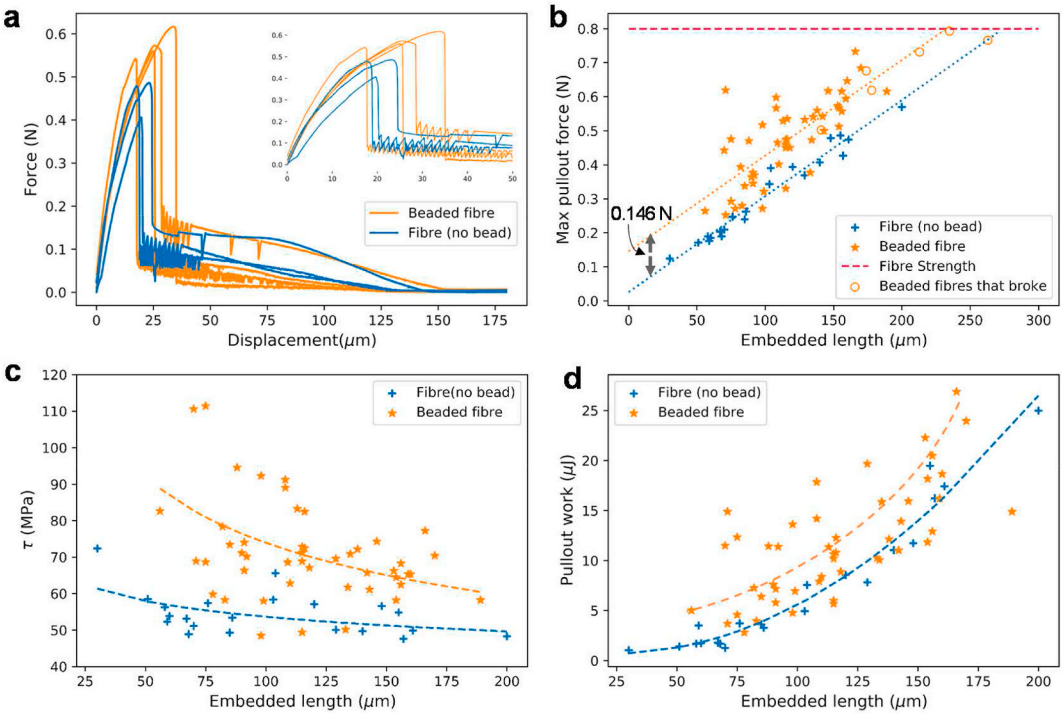


**Fig. 6. Comparison of pullout behaviour between beaded fibres (orange) and beadless fibres (blue)**. (a) Force-displacement graphs at embedded length of 145 ± 10 µm. (b) Maximum pullout force vs. embedded length. The dotted lines are linear fits to the data. Beaded fibres that broke are marked separately. The horizontal dashed line indicates the limit above which the fibres broke rather than pulled out. (c) Interfacial shear strength vs. embedded length, calculated using Equation (1). The dashed lines are power fits to the data. (d) Pullout work vs. embedded length. Trendlines are depicted as dashed curves. (For interpretation of the references to colour in this figure legend, the reader is referred to the Web version of this article.)

For beaded fibres, $d$ was taken as the fibre diameter only, without considering the bead diameter (Fig. 1). The effective interfacial shear strength of the beaded fibres was higher than that of the beadless fibres for most beaded samples. In beaded samples, $\tau$ was seen to increase significantly at shorter embedded lengths as the bead interface gets larger with respect to the matrix interface.

The shortest embedded length possible for beaded fibres was ~55 μm. At this embedded length, $\tau_{beaded\ fibre}$ was calculated to be 89 MPa. For the control fibre (without bead) at the same embedded length, $\tau_{fibre\ (no\ bead)}$ was calculated to be 57 MPa. At the longest possible embedded length of 200 μm, $\tau_{beaded\ fibre} = 59$ MPa and $\tau_{fibre\ (no\ bead)} = 49$ MPa. These values were extracted from the fitting curves in Fig. 6c at embedded lengths of 55 μm and 200 μm, respectively. The average $\tau_{fibre\ (no\ bead)}$ (the IFSS) was calculated from the slope of the fitting curve in Fig. 6b to be 52.4 MPa. The presence of the bead increased the effective interfacial shear strength of a fibre and this increase was seen to be more pronounced at shorter embedded lengths. The pullout work (*i.e.*, area under the force displacement graph) vs. the embedded length for beaded fibres is shown in Fig. 6d. Most beaded fibre samples either had higher pullout work for a given embedded length than beadless fibres or the pullout work remained the same as the control. Again, a larger scatter was observed for the pullout data from the beaded fibres as compared to the beadless fibres. The results from the single fibre pullout tests therefore imply that there is a simultaneous increase in fibre anchorage and energy dissipation due to the presence of the bead at the fibre-matrix interface.

### 3.4. Effect of bead diameter on pullout

Fig. 7a shows the dependence of the force and pullout work on bead diameter, by mapping the experimental data (dots) into contour maps (curves) for rising values of embedded length; because the data is scattered, the contour lines are smoothed. As seen, a moderate increase in both the force and work was observed when the bead diameter decreased. At first glance this may seem counter-intuitive, as one would think that larger beads would offer a greater obstacle to pullout. However, thicker beads spread the radial force over a longer circumference, and consequently reduce the stress transmitted to the fibre. Conversely, the pressure transmitted to the fibre through thinner beads is higher, creating a stronger mechanical locking effect. The bead aspect ratio (length/diameter) is an important indicator for these trends (Fig. 7b). This is explained further in section 3.7 which deals with the pullout mechanism.

### 3.5. Effect of cure cycle on the properties of bead

The simultaneous increase in pullout force and work of single beaded fibres is a surprising result, given that the bead was not pulled out from the matrix for any of the samples, and that the bead and the matrix were of the same material. The bead, however, underwent a second curing cycle while preparing samples for the pullout test: it first was cured at 6 h at 100 °C to form the beads on the fibre, then was left to stand at room temperature for 24 h before being embedded into the matrix and cured for another 6 h at 100 °C. Therefore, we had to ask the question as to whether or not the simultaneous increase in interfacial shear strength and pullout work, seen in section 3.3, was simply due to the bead having a different curing degree from the rest of the matrix. A difference in curing degree has been known to alter the mechanical properties of a polymer [26].

Ideally, a direct method of testing the effects of the cure cycle on the pullout results would be to coat and cure a thin layer of epoxy onto a fibre before embedding it in bulk epoxy and performing a pullout test. Practically, however, this is not possible, as beads form spontaneously on the surface of a fibre even when a thin layer of epoxy is deposited on it, due to the Plateau-Rayleigh instability. Therefore, instead, bulk epoxy characterisation tests were performed to understand the effects of the cure cycle on epoxy properties. The epoxy beads themselves were too small for direct characterisation tests and so the tests were carried out on bulk epoxy, with the same cure conditions as the bead and as the epoxy matrix. Two batches of epoxy were made, as described in section 2.5. The first batch that was cured only once was labelled SCE (single cure epoxy) and was used to emulate the cure condition of the matrix. The second batch that was cured twice emulated the cure condition of the bead in the pullout test and was labelled as DCE (double cure epoxy).

#### 3.5.1. Curing degree and glass transition temperature

DSC scans of SCE and DCE with their respective glass transition temperatures ($T_g$) are seen in Fig. 8. The $T_g$ is the temperature at which a polymer transitions between a glassy, more crystallised state and a rubbery amorphous state. A number of factors influence a polymer's $T_g$, such as degree of cure and the cure time and temperature [26].

DSC analysis first proved that the epoxy was fully cured after a single curing cycle (SCE). Had the epoxy not been fully cured, an exothermic peak would have been present in the DSC scan shortly after the $T_g$ [26]. As seen in Fig. 8, an exothermic curing peak is absent in the DSC scan of SCE. The DCE sample had a slightly higher $T_g$ (80.2 °C) compared to the SCE sample (77.6 °C). This indicated that there was no thermal

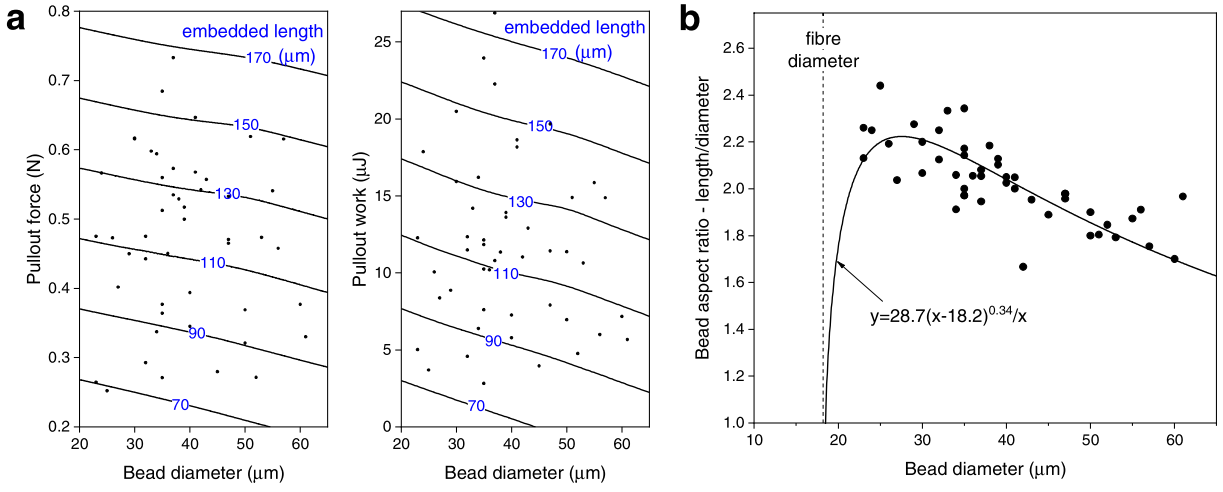


**Fig. 7. Effect of bead diameter on pullout force and work.** (a) Contour maps (smoothed) of the experimental pullout force and work vs. the bead diameter, for a range of embedded lengths. The dots indicate the experimental data used to create the maps. (b) Bead aspect ratio (length/diameter) vs. the bead diameter. The fitting curve and equation are shown, with extrapolation to smaller bead diameters converging towards fibre diameter. The dataset is the same as in Fig. 6.

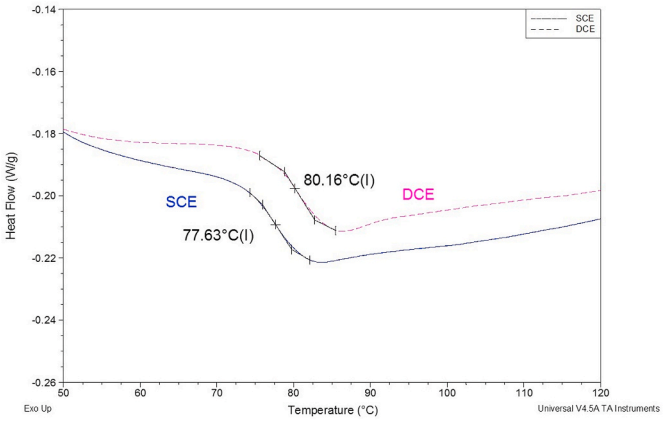


**Fig. 8. Differential scanning calorimetry (DSC) of bead and matrix samples**. Showing slight increase in $T_g$ of DCE (double cure epoxy) as compared to SCE (single cure epoxy).

degradation in the epoxy on undergoing a second cure and instead pointed to a possible improvement in the mechanical properties of the epoxy. Thermal degradation is usually accompanied by a decrease in the $T_g$ of a polymer and a degradation in the mechanical properties of a polymer. Inversely, an increase in $T_g$ usually accompanies an improvement in the mechanical properties of a polymer [26]. Mechanical tests were therefore performed on SCE and DCE samples to investigate this further.

### 3.5.2. Bulk epoxy strength and stiffness

Bulk epoxy tensile tests were performed on dog-bone shaped coupons of SCE and DCE samples, as described in section 2.5.1. 10 coupons were tested for sample and the results are presented in Table 2.

The mechanical properties of SCE and DCE samples did not differ significantly from each other, implying that the cure cycle had negligible effect on the mechanical properties of epoxy. Thus, it is improbable that the curing degree of the bead and matrix was the cause for the increased pullout force and work of the beaded fibres seen in section 3.3.

### 3.5.3. Effect of cure cycle on fibre-matrix interfacial properties

The second cure cycle did not affect the mechanical properties of the epoxy, but perhaps it affected the interfacial properties instead. Pullout tests were therefore performed using beadless fibres embedded in epoxy that had gone through a cure cycle twice (DCE). The fibres were embedded in liquid epoxy and cured once, as described in section 2.4.1. On completing the first cure cycle, the samples were removed from the oven and left to stand at room temperature for 24 h. They were then reinserted into an oven and heated at 100 °C for another 6 h. Pullout tests were then performed and the results were compared to the pullout of fibres from epoxy that was cured only once (the control for this section; labelled SCE). Significant overlap was seen between the data points of the DCE pullout tests and SCE (Fig. 9).

When analysing $\tau_{DCE}$ using Equation (1), an average value of 59 ± 6 MPa was obtained. $\tau_{SCE}$ was calculated to be 54 ± 6 MPa. However, on performing a T-test on the values of $\tau$ for each sample ($\tau$ calculated using Equation (1)), a p-value of 0.06 was obtained, implying that there was no significant difference between $\tau_{DCE}$ and $\tau_{SCE}$. Thus, the cure cycle of the epoxy did not significantly affect the interfacial properties of the fibre-matrix system. It could therefore be concluded from the characterisation tests in this section, that the simultaneous increase in both pullout work and pullout force (and consequently, interfacial shear strength) was not due to a change in material property of the bead. This conclusion led us to explore different mechanisms related to, perhaps, geometrical conformation instead of material properties.

### 3.6. Pullout debonding morphology

Micro-computer tomography (μCT) scans were performed on the matrices of samples after the pullout test (Fig. 10). Fig. 10a shows the scan of a beadless fibre (the control), and Fig. 10b shows the scan of a beaded fibre sample after pullout at the same embedded length (75 μm). The bead itself could not be seen in the μCT scan because it is of the same material as the matrix, but its position before and after pullout is marked in Fig. 10b. A large conical void was observed in the matrix of the beaded fibre, not seen in the matrix of the control. μCT scans enhance the contrast of boundaries, particularly at material gaps, and therefore the void seems to be the result of relative displacement between the fibre, bead and matrix components. Thus, the void is likely due to the fibre and bead ends debonding from the matrix, and their consequent travelling some distance inside the matrix before bead-fibre interface failure and fibre pullout, as shown in the schematic Fig. 10d. Similar possible debonding at the boundary of the bead front half could not be detected by the μCT scan as the high pressure between the bead and the matrix eliminated the feasibility of a gap. A variation observed in void size for each sample may also be contributing to the scatter seen in the data in section 3.3. The debonding of the back end of the bead is not thought be along the entire back end, but more along a smaller section close to the fibre end. Any boundary of the section debonded, therefore, is very likely masked by the much larger conical void left in the matrix behind the bead as it pushes through the matrix during pullout.

The presence of this void in the matrix implies that the bead is not perfectly bonded to the matrix. If the bead were perfectly bonded, then, in view of the identical mechanical properties of the bead and the matrix, there would not have been any change in the behaviour between beaded and beadless fibres. We can therefore assess that the bead-matrix bonding is weaker that the bulk epoxy. From the DSC analysis in section 3.5.1, it is seen that the bead was fully cured after the first cure cycle. Upon embedding and curing in the epoxy matrix, less crosslinks would form between the fully cured bead and the matrix compared to the crosslinks within the bulk epoxy matrix itself. We may consequently expect some relative motion between the adjacent contact surfaces of the bead and the matrix.

### 3.7. Pullout mechanism and phenomenological model

Since the bead and matrix are made of identical materials to form a unified structure with uniform mechanical properties, the question then arises as to why we observe a higher pullout force in the beaded fibres compared to beadless ones? A straight-forward explanation is the possible effect of the bead's double-curing, which might enhance healing or bridging of fibre flaws, might increase bead strength, or might increase matrix thermal shrinkage. However, these mechanisms should be rejected because, as observed, the strength and stiffness of the bead and embedding matrix were found to be essentially the same (Table 2 and Fig. 9). Furthermore, in such mechanisms, the pullout force and work would be decreased when decreasing the bead size, rather than

**Table 2**
Epoxy tensile tests and measured stiffness, strain and strength.

| | Epoxy cured once (SCE) | Epoxy cured twice (DCE) | p-value (T-Test) |
|---|---|---|---|
| Modulus | 1.80 ± 0.16 | 1.85 ± 0.13 | 0.43 |
| Strain-to-failure (%) | 13.4 ± 1.5 | 13.1 ± 2.7 | 0.93 |
| Tensile Strength (MPa) | 64.7 ± 2.6 | 64.4 ± 1.2 | 0.79 |

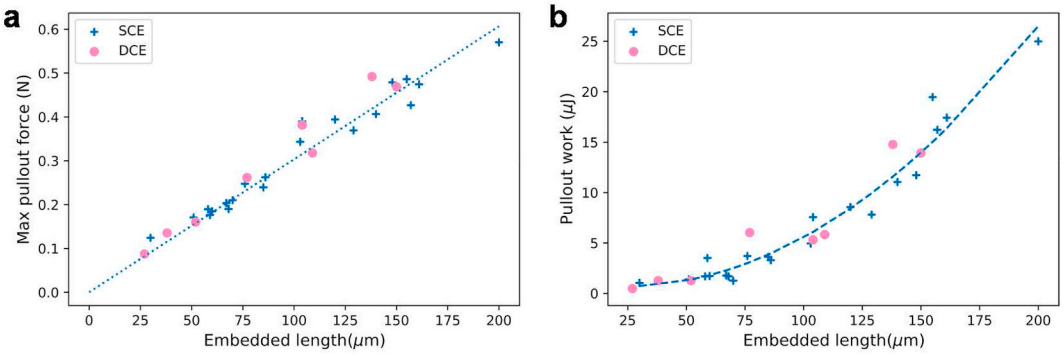


**Fig. 9. Pullout from double cure epoxy (DCE) compared to single cure epoxy (SCE).** (a) Pullout force. (b) Pullout work.

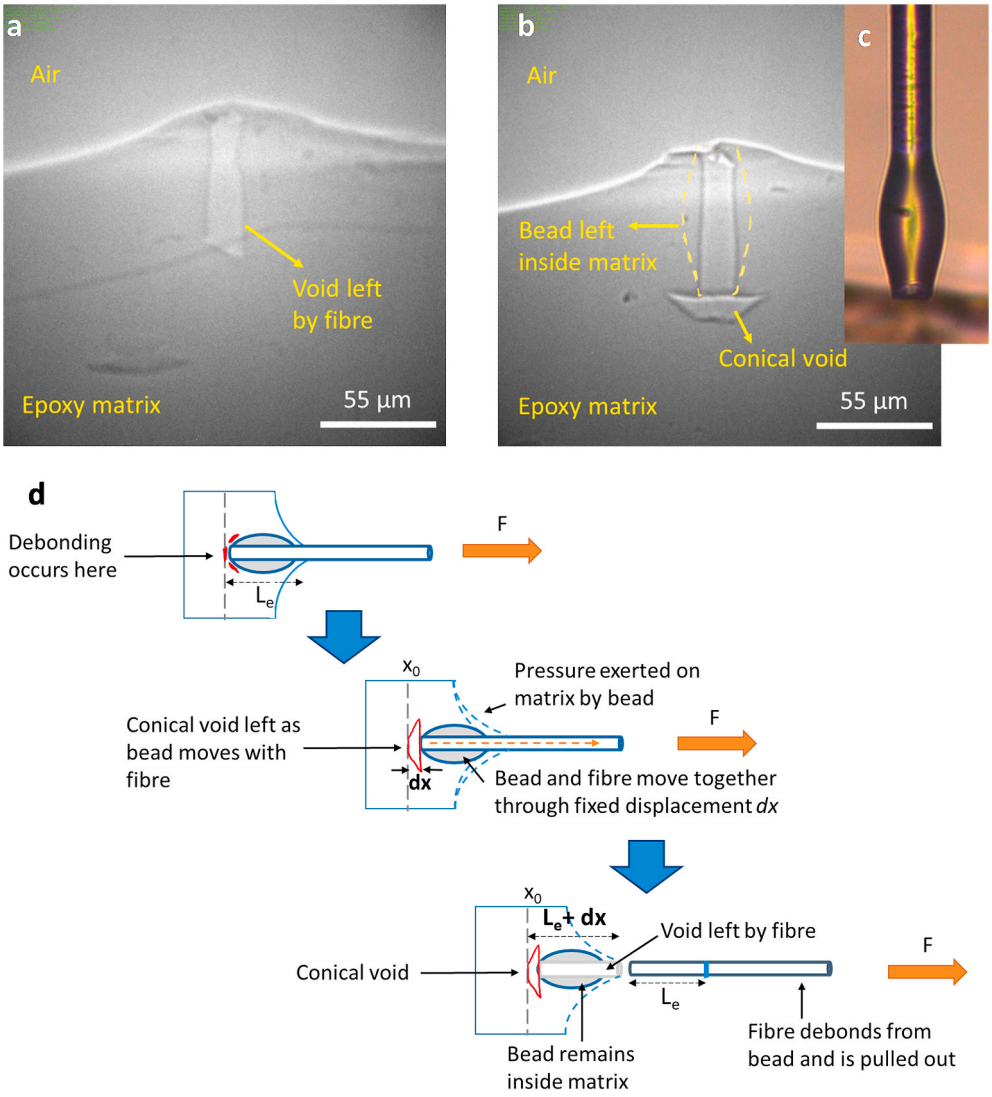


**Fig. 10. Computed tomography scans of matrices after pullout test**. (a) Scan of control (b) Scan of beaded fibre. (c) Bead before embedding in matrix (d) Illustration of pullout mechanism. $L_e = 75$ μm, $dx = 10$ μm.

increased as seen in our observations (Fig. 7a). By contrast, a mechanism based on bead-matrix interface debonding seems consistent with the observations (Fig. 11a).

The mechanism proposed is based on mechanical locking of the fibre by friction (herein termed 'friction lock'). Under a pullout force, the stress exerted by the matrix on the bead is converted to radial pressure, which propagates through the bead to the fibre interface (Fig. 11b). The ensuing pressure on the fibre induces a friction shear stress ($\tau_f$), which adds up to the matrix bonding stress ($\tau_i$) (Fig. 11c). For this to happen, we assume that the bead debonds from the matrix prior to fibre pullout, and that the bead front half (the side facing the load) presses against the matrix via a tapered interface with friction (Fig. 10 and ref. [14]). We

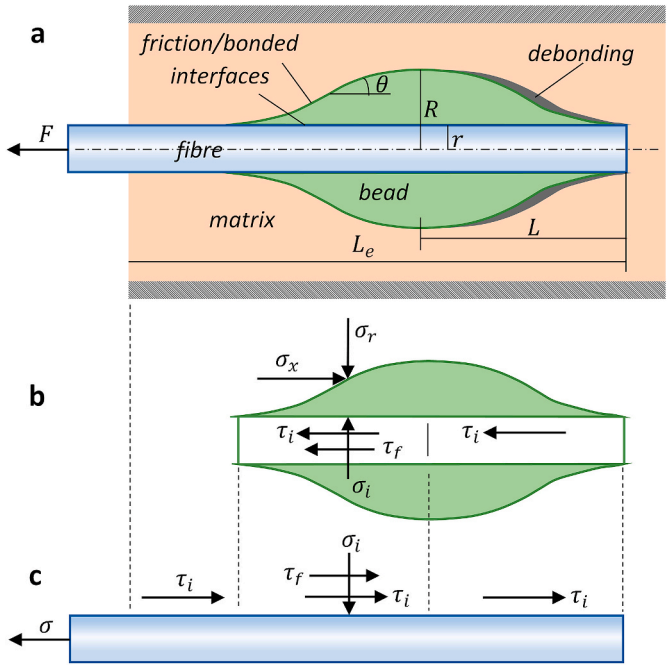


**Fig. 11. Beaded fibre pullout model.** (a) Model components, interfaces and geometry. (b) Stresses on the bead. (c) Stresses on the fibre. $\sigma$ is the pullout stress applied to the fibre, $\sigma_x$ and $\sigma_r$ are reaction stresses applied by the matrix on the bead, $\sigma_i$ is the radial pressure between the bead and the fibre due to bead radial compression, $\tau_i$ is the bonding shear strength of the matrix-fibre interface, and $\tau_f$ is the matrix-fibre friction shear stress due to the radial pressure. Note: the forces are denoted the same as the stresses by replacing $\sigma$ by $F$.

further assume, as in the classic Cottrell-Kelly-Tyson (CKT) model [22–24,27], that at the time of fibre pullout the matrix material at the fibre interface yields and flows plastically, maintaining a constant stress equal to the matrix yield strength in shear; this assumption is supported by the observed segment of plastic travel during pullout (Fig. 6a).

The debonding and friction premise should be regarded as a conceptual mechanism, which captures the effects of the relative displacement between the bead and matrix contact surfaces, as well as between the bead and fibre contact surfaces. The actual physical mechanism can be a combination of contact friction and elastic and plastic deformations, the description of which is beyond the present scope. So, the friction mechanism in our modelling is viewed as a conceptual envelope for this combination of effects, and in that respect our model is phenomenological.

Consider the stresses acting on the bead as a result of fibre tension (Fig. 11b). At the bead-fibre interface, the shear stresses exerted by the fibre include: (i) a bonding interfacial stress $\tau_i$, assumed uniform and equal to the matrix material yield strength, which acts throughout the bead length $2L$ and generates a force $4\pi rL\tau_i$, and (ii) a mean friction stress $\tau_f$, caused by the radial pressure between the bead and the fibre, which is assumed to act just on the bead front half $L$ and generates a force $2\pi rL\tau_f$. The reaction stresses, exerted by the matrix on the front slope of the bead, are proportional to the sum of these forces, $2\pi rL(2\tau_i + \tau_f)$, and so

$$\sigma_r \propto 2\tau_i + \tau_f \tag{2}$$

which depends on the bead slope $\theta$ and the friction. The radial pressure induced by $\sigma_r$ propagates through the bead toward the fibre, much like in a pressure vessel under external pressure, with a proportional radial reaction $\sigma_i \propto \sigma_r$. The friction stress at the bead-fibre interface is proportional to that reaction, that is $\tau_f \propto \sigma_i \propto \sigma_r \propto 2\tau_i + \tau_f$. Introducing a proportionality factor $\alpha$, this becomes:

$$\tau_f = \alpha(2\tau_i + \tau_f) \tag{3}$$

where $\alpha$ ($0 \le \alpha < 1$) is a dimensionless factor that captures the friction at both contact surfaces of the bead, the slope of the bead slant surface, and the elastic transmission of the radial stress through the bead. Note that $\tau_f$ appears on both sides of the equation, because when it is higher the radial pressure is higher, further increasing its value in a self-enhancing cycle. For a given bead size and shape and friction coefficients, $\alpha$ is constant. The mean friction shear stress as a function of the bonding shear stress is thus

$$\tau_f = \frac{2\alpha}{1-\alpha}\tau_i \tag{4}$$

Because the local thickness and angle of the bead slope vary along its length, the radial pressure and friction stress vary as well, and therefore $\tau_f$ is a mean stress. We see that as $\alpha$ gets higher the friction stress increases, and when $\alpha \to 1$ the friction stress diverges, and consequently the fibre will not pull out but instead break. The condition for such a lock is thus $\alpha_{\text{lock}} = 1$. As the lock is brought about by the interplay between the friction stresses at the bead-matrix and bead-fibre contact surfaces, we term this mechanism 'friction lock'. This effect resembles the action of a tapered key or wedge pressed between mechanical parts in order to lock them together via friction, for example, a tapered key pressed between a shaft and a wheel thereby locking them mechanically together.

The contribution of the friction lock to the pullout force is

$$F_f = 2\pi rL\tau_f = \frac{4\pi rL\alpha}{1-\alpha}\tau_i \tag{5}$$

Using average experimental values, $F_f = 0.146$ N (Fig. 6b), $\tau_i = 52.4$ MPa, $r = 9.1$ μm, and $2L = 78.8$ μm, we get the fitting value $\alpha_{fit} \cong 0.382$. The corresponding friction shear stress is $\tau_f \cong 1.24\tau_i \cong 64.8$ MPa (Equation (4)). We see that, in our experiments, the magnitude of the friction shear stress was high, comparable to or even higher than the bonding shear strength. Evidently, if the resulting pullout stress is higher than the fibre strength, the fibre will break rather than pull out. If the fibre remains bonded to the bead and the pullout force exceeds the maximum force the matrix can bear, the bead will pull out from the matrix by shearing or compressing it. To obtain the pullout force when the fibre pulls out, the bonding shear force along the full embedded length of the fibre, $2\pi rL_e\tau_i$, is added to $F_f$:

$$F = 2\pi r(L_e\tau_i + L\tau_f) = 2\pi r\left(L_e + \frac{2\alpha}{1-\alpha}L\right)\tau_i \tag{6}$$

Equation (5) teaches us that the friction lock contribution depends on the bead half-length $L$ and the factor $\alpha$, and, as observed, is constant for a given bead shape, size and contacts friction. To understand the bead size effect, particularly to explain why the pullout force and work are seen to rise moderately with decreasing bead diameter (Fig. 7a), we resort to the following scaling analysis. The radial force exerted by the matrix on the bead is spread over the bead mean circumference. Therefore, when the bead radius $R$ is smaller, the circumference is shorter and the resultant radial stress $\sigma_r$ is higher, leading to scaling $\sigma_r \propto R^{-1}$. This stress remains fairly constant across the bead thickness because of the reaction $\sigma_i$ exerted by the (rigid) fibre, similar to the constant stress in a solid cylinder under external pressure. Thus, $\sigma_i \approx \sigma_r \propto R^{-1}$ and consequently $\tau_f \propto \sigma_i \propto R^{-1}$. This leads to the following scaling relationship for the friction-added pullout force, $F_f \propto L\tau_f \propto L/R$ (Equation (5)). That is, the friction lock contribution to the pullout force is proportional to the bead aspect ratio, such that a longer bead provides longer friction surface, while a thinner bead provides higher pressure, both contributing to a higher friction force, and vice versa. Similarly, because the pullout travel prior to fibre debonding is proportional to $F_f$, the friction lock contribution to the pullout work should scale as $W_f \propto {F_f}^2 \propto (L/R)^2$.

Using the fitting approximation for $L/R$ in Fig. 7b (based on bead modeling [14,15]), the force (and similarly the work) can be expressed

in terms of the radii, $F_f \propto (R-r)^{\nu}/R$ where $\nu \cong 0.34$. This force function has a maxima at bead radius $R = r/(1-\nu) \cong 1.5r$, above which $F_f$ decreases moderately, but below which $F_f$ drops sharply to zero. This drop is expected, as the locking effect should vanish when the bead diameter approaches the fiber diameter (that is, the bead almost disappears). The measured bead dimensions in Fig. 7b indeed show a moderate rise of the aspect ratio $L/R$ (and therefore of $F_f$ and $W_f$) for decreasing bead diameter, and predicts that after reaching a peak it drops steeply toward zero. The corresponding peak pullout force and work can be regarded as design points for possible optimal strength and toughness. The maximum friction-lock force or work is reached at a bead diameter quite close to the fibre diameter, and further diameter reduction may eventually result in bead pull out from the matrix and loosening of the anchoring effect.

To summarize: (1) the theoretical model explains the rise of the pullout force and work for beaded fibres as a self-locking friction mechanism; (2) the model agrees well with the results of our pullout experiments; (3) the pullout force and work are found to increase for smaller beads, allowing compact packing of multiple beaded fibres in a practical composite.

## 4. Conclusion

Geometrical modifications of the fibre-matrix interface appear to be a promising way forward to simultaneous increase in strength and toughness in composites, as seen in the current study of single beaded fibres. Single fibre pullout tests of fibres beaded with epoxy droplets showed a simultaneous increase in pullout force and work, implying that the presence of the bead enhanced the anchoring and energy dissipation of a fibre during pullout from a matrix. The bead and the matrix were made from the same material, and characterisation tests revealed that their mechanical and material properties did not differ significantly; therefore, this enhancement in pullout behaviour was unexpected. Furthermore, the bead was not pulled out along with the fibre during pullout, but remained in the matrix. μCT scans taken of the matrix after pullout suggested that the bead and the matrix did not act as a solid entity, but rather that partial debonding possibly occurred between the bead and the matrix when under load. This hypothesis was in line with the observations in our previous work [14].

A conceptual friction lock mechanism was proposed in which it is assumed that during pullout, partial debonding occurs between the bead and the matrix. Pressure exerted by the matrix as the bead pushes against the matrix is transmitted radially through the bead to the bead-fibre interface, inducing a friction stress that contributes to the shear stress at the interface. The phenomenological model based on this hypothesised mechanism agrees well with the experimental data. It was found that pullout force and work increased for smaller beads, which is beneficial for practical applications of beaded fibres in real composites as it allows compact packing of multiple beaded fibres towards realistic volume fractions.

In this study, we limited ourselves to using epoxy beads that were chemically and physically identical to the matrix and it was seen that, to a certain extent, the interfacial shear strength and pullout work of the model could be tuned using different bead sizes. The system has further potential for tuning if, for instance, different materials are used for the bead and the matrix, as was mentioned in our previous work [15]. Further tests are anticipated in this direction, and in the direction of multi-beaded fibre composites.

## Author statement

**Carol W. Rodricks:** Conceptualization, Methodology, Investigation, Visualization, Writing - Original Draft, Writing - Review and Editing. **Israel Greenfeld:** Conceptualization, Formal analysis, Visualization, Writing - Original Draft, Writing - Review and Editing. **H. Daniel Wagner:** Conceptualization, Supervision, Writing - Review and Editing.

## Declaration of competing interest

The authors declare that they have no known competing financial interests or personal relationships that could have appeared to influence the work reported in this paper.

## Acknowledgements

The authors would like to acknowledge support from the G.M.J. Schmidt Minerva Centre of Supramolecular Architectures at the Weizmann Institute, and the generosity of the Harold Perlman family. C.W.R. was supported by the European Union's Horizon 2020 research and innovation ITN programme under the Marie Sklodowska-Curie grant agreement No 722626 FiBreMoD. This research was supported in part by the Israel Science Foundation (grant #2439/19). The authors would like to acknowledge Dr Sergey Kapishnikov from the Department of Chemical Research Support at the Weizmann Institute of Science for his help in attaining μCT images. H.D.W. is the recipient of the Livio Norzi Professorial Chair in Materials Science.

## References

[1] R.O. Ritchie, The conflicts between strength and toughness, Nat. Mater. 10 (11) (2011) 817–822, https://doi.org/10.1038/nmat3115.
[2] U.G.K. Wegst, H. Bai, E. Saiz, A.P. Tomsia, R.O. Ritchie, Bioinspired structural materials, Nat. Mater. 14 (1) (2015) 23–36, https://doi.org/10.1038/nmat4089.
[3] S. Fu, B. Zhou, C. Lung, On the pull-out of fibres with a branched structure and the inference of strength and fracture toughness of composites, Compos. Sci. Technol. 47 (3) (Jan. 1993) 245–250, https://doi.org/10.1016/0266-3538(93)90033-D.
[4] P.S. Chua, M.R. Piggott, The glass fibre-polymer interface: I-theoretical consideration for single fibre pull-out tests, Compos. Sci. Technol. 22 (1) (1985) 33–42, https://doi.org/10.1016/0266-3538(85)90089-2.
[5] M. Tanoglu, S.H. McKnight, G.R. Palmese, J.W. Gillespie, Effects of glass-fiber sizings on the strength and energy absorption of the fiber/matrix interphase under high loading rates, Compos. Sci. Technol. 61 (2) (2001) 205–220, https://doi.org/10.1016/S0266-3538(00)00195-0.
[6] J.K. Kim. Engineered Interfaces in Fiber Reinforced Composites, first ed., Elsevier, Amsterdam, 1998,. https://doi.org/10.1016/B978-008042695-2/50006-3.
[7] W. Liu, et al., Improvement in interfacial shear strength and fracture toughness for carbon fiber reinforced epoxy composite by fiber sizing, Polymer Composites 35 (3) (2013). https://doi.org/10.1002/pc.22685.
[8] F. Barthelat, Z. Yin, M.J. Buehler, Structure and mechanics of interfaces in biological materials, Nature Publishing Group, Nat. Rev. Mater. 1 (4) (2016) 1–16, https://doi.org/10.1038/natrevmats.2016.7. Mar. 08.
[9] S.E. Naleway, M.M. Porter, J. McKittrick, M.A. Meyers, Structural design elements in biological materials: application to bioinspiration, Adv. Mater. 27 (37) (Oct. 2015) 5455–5476, https://doi.org/10.1002/adma.201502403.
[10] F. Barthelat, H.D. Espinosa, An experimental investigation of deformation and fracture of nacre-mother of pearl, Exp. Mech. 47 (3) (2007) 311–324, https://doi.org/10.1007/s11340-007-9040-1.
[11] A.M. Torres, et al., Bone-inspired Microarchitectures Achieve Enhanced Fatigue Life, PNAS 116 (49) (2019), https://doi.org/10.1073/pnas.1905814116.
[12] T. Lingham-Soliar, R.H.C. Bonser, J. Wesley-Smith, Selective biodegradation of keratin matrix in feather rachis reveals classic bioengineering, Proc. R. Soc. B Biol. Sci. 277 (1685) (2010) 1161–1168, https://doi.org/10.1098/rspb.2009.1980.
[13] C.M. Laurent, C. Palmer, R.P. Boardman, G. Dyke, R.B. Cook, Nanomechanical properties of bird feather rachises: exploring naturally occurring fibre reinforced laminar composites, J. R. Soc. Interface 11 (101) (Dec. 2014) 20140961, https://doi.org/10.1098/rsif.2014.0961.
[14] I. Greenfeld, W. Zhang, X.M. Sui, H.D. Wagner, Intermittent beading in fiber composites, Compos. Sci. Technol. 160 (2018) 21–31, https://doi.org/10.1016/j.compscitech.2018.03.003.
[15] I. Greenfeld, C.W. Rodricks, X. Sui, H.D. Wagner, Beaded fiber composites—stiffness and strength modeling, J. Mech. Phys. Solid. 125 (Apr. 2019) 384–400, https://doi.org/10.1016/j.jmps.2018.12.020.
[16] R.C. Wetherhold, F.K. Lee, Shaped ductile fibers to improve the toughness of epoxy-matrix composites, Compos. Sci. Technol. 61 (4) (2001) 517–530, https://doi.org/10.1016/S0266-3538(00)00217-7.
[17] R.C. Wetherhold, M. Corjon, P.K. Das, Multiscale considerations for interface engineering to improve fracture toughness of ductile fiber/thermoset matrix composites, Compos. Sci. Technol. 67 (11–12) (2007) 2428–2437, https://doi.org/10.1016/j.compscitech.2007.01.004.
[18] Y.T. Zhu, I.J. Beyerlein, Bone-shaped short fiber composites — an overview, Mater. Sci. Eng., A 326 (2002) 208–227, https://doi.org/10.1016/s0921-5093(01)01486-1.

[19] Humburg H., Zhu D., Beznia S., Barthelat F., Bio-inspired tapered fibers for composites with superior toughness, Compos. Sci. Technol. 72 (9) 1012–1019. https://doi.org/10.1016/j.compscitech.2012.03.013.
[20] J.J. Blaker, et al., Property and shape modulation of carbon fibers using lasers, ACS Appl. Mater. Interfaces 8 (25) (2016) 16351–16358, https://doi.org/10.1021/acsami.6b05228.
[21] C. Yang, R. Han, M. Nie, Q. Wang, Interfacial reinforcement mechanism in poly (lactic acid)/natural fiber biocomposites featuring ZnO nanowires at the interface, Mater. Des. 186 (Jan. 2020) 108332, https://doi.org/10.1016/j.matdes.2019.108332.
[22] A.H. Cottrell, Strong solids, Proc. R. Soc. A Math. Phys. Eng. Sci. 282 (1388) (1964) 2–9, https://doi.org/10.1098/rspa.1964.0206.
[23] A. Kelly, Interface effects and the work of fracture of a fibrous composite, Proc. R. Soc. London. Ser. A, Math. Phys. Sci., vol. 319, no. 1536, pp. 95–116, https://doi.org/10.1098/rspa.1970.0168.
[24] A. Kelly, W.R. Tyson, Tensile properties of fibre-reinforced metals: copper/tungsten and copper/molybdenum, J. Mech. Phys. Solid. 13 (6) (1965) 329–350, https://doi.org/10.1016/0022-5096(65)90035-9.
[25] Z. Wang, et al., An effective method to improve the interfacial shear strength in GF/CF reinforced epoxy composites characterized by fiber pull-out test, Compos. Commun. 19 (2020) 168–172, https://doi.org/10.1016/j.coco.2020.03.013. February.
[26] R.J.C. Carbas, E.A.S. Marques, L.F.M. Da Silva, A.M. Lopes, Effect of cure temperature on the glass transition temperature and mechanical properties of epoxy adhesives, J. Adhesion, Jan. 90 (1) (2014) 104–119, https://doi.org/10.1080/00218464.2013.779559.
[27] I. Greenfeld, H.D. Wagner, Nanocomposite toughness, strength and stiffness: role of filler geometry, Nanocomposites 1 (1) (2015) 3–17, https://doi.org/10.1179/2055033214Y.0000000002.